

# Electric-Field-Induced Orientation of Surfactant-Templated Nanoscopic Silica

Anthony Y. Ku,<sup>†</sup> Dudley A. Saville,<sup>‡</sup> and Ilhan A. Aksay\*

Department of Chemical Engineering, Princeton University, Princeton, New Jersey 08544

Received December 14, 2006. In Final Form: April 9, 2007

While exhibiting a well-defined nanometer-level structure, surfactant-templated nanoscopic silicas produced via self-assembly do not always possess long-range order. We demonstrate that long-range order can be controlled by guiding the self-assembly of nanostructured silica-surfactant hybrids with low-strength electric fields ( $E \sim 200$  V/m) to produce nanoscopic silica with both the micrometer- and nanometer-level structures oriented parallel to the applied field. Under the influence of the electric field, nanoscopic silica particles migrate, elongate, and merge into fibers with a rate of migration proportional to the applied field strength. The linear dependence with the field strength indicates that the process is governed by electroosmotic flow but not by polarization effects. Realignment of the short-range ordered surfactant nanochannels along the fiber axis accompanies the migration.

## Introduction

The well-packed, tunable, monodisperse channel structure in nanoscopic silica produced through the self-assembly of surfactants holds great promise for applications ranging from microelectronics to environmental and biological separations to catalytic hosts.<sup>1–10</sup> In the system discussed in this work, the synthesis involves mixing a silicate precursor into an acidified surfactant micelle solution to form a nanostructured hybrid material consisting of hexagonally packed surfactant tubules within the silica.<sup>1,2,11</sup> Following synthesis, the surfactant can be removed via calcination, solvent reflux, or ion exchange to leave behind a nanoporous inorganic network. While self-assembly is an excellent method for producing short-range order, its ability to produce long-range orientation is limited. Consequently, nanoscopic silica films and particles often contain channels that are curved, oriented parallel to the surface, and organized into multiple domains, which are ill-suited for use in porous media applications due to the disruption of channel continuity.<sup>12–14</sup>

One way to control the long-range orientation and thus channel continuity is to guide the self-assembly process using van der Waals anisotropy,<sup>12,15</sup> surface registry effects,<sup>16,17</sup> physical confinement,<sup>16,18–21</sup> shear flows,<sup>16,22–26</sup> magnetic fields,<sup>27,28</sup> electric fields,<sup>18</sup> and combinations thereof.<sup>12,18,24</sup> However, orientation effected via van der Waals anisotropy, surface registry, and confinement effects is limited to in-plane directions. Flow fields offer greater degrees of flexibility in the orientation, but high shear rates are often required, which limit the size of the structures that can be prepared. Magnetic and electric fields offer flexibility in the orientation and can be applied over large areas, but, until now, high field strengths ( $10^8$  V/m) have been used.<sup>18</sup>

Electric fields present an intriguing option because they are tunable, scalable, and capable of producing orientation in different geometries. Electric fields interact with materials through two mechanisms. In dielectric materials, they give rise to *induced dipole (polarization) effects*, which have been used to align the equilibrium structure of microphase-separated block copolymers<sup>29,30</sup> as well as guide structure formation in reacting polymer

\* Corresponding author. Telephone: 609-258-4393. E-mail: iaksay@princeton.edu.

<sup>†</sup> Present address: General Electric, Global Research Center, Niskayuna, NY 12309.

<sup>‡</sup> Deceased, October 4, 2006.

(1) Kresge, C. T.; Leonowicz, M. E.; Roth, W. J.; Vartuli, J. C.; Beck, J. S. *Nature* **1992**, *359*, 710–712.

(2) Huo, Q.; Margolese, D. I.; Ciesla, U.; Feng, P.; Gier, T. E.; Sieger, P.; Leon, R.; Petroff, P. M.; Schüth, F.; Stucky, G. D. *Nature* **1994**, *368*, 317–321.

(3) Yang, P.; Zhao, D.; Margolese, D. I.; Chmelka, B. F.; Stucky, G. D. *Chem. Mater.* **1999**, *11*, 2813–2826.

(4) Brinker, C. J.; Lu, Y.; Sellinger, A.; Fan, H. *Adv. Mater.* **1999**, *11*, 579–585.

(5) Baskaran, S.; Liu, J.; Domansky, K.; Kohler, N.; Li, X.; Coyle, C.; Fryxell, G. E.; Thevuthasan, S.; Williford, R. E. *Adv. Mater.* **2000**, *12*, 291–294.

(6) Yang, P.; Wirthsberger, G.; Huang, H. C.; Cordero, S. R.; McGehee, M. D.; Scott, B.; Deng, T.; Whitesides, G. M.; Chmelka, B. F.; Buratto, S. K.; Stucky, G. D. *Science* **2000**, *287*, 465–467.

(7) Nguyen, T. Q.; Wu, J.; Doan, V.; Schwartz, B. J.; Tolbert, S. H. *Science* **2000**, *288*, 652–656.

(8) Feng, X.; Fryxell, G. E.; Wang, L. Q.; Kim, A. Y.; Liu, J.; Kemner, K. M. *Science* **1997**, *276*, 923–925.

(9) Hata, H.; Saeki, S.; Kimura, T.; Sugahara, Y.; Kuroda, K. *Chem. Mater.* **1999**, *11*, 1110–1119.

(10) Maschmeyer, T. *Curr. Opin. Solid State Mater.* **1998**, *3*, 71–78.

(11) Brinker, C. J.; Scherer, G. W. *Sol–Gel Science*; Academic Press: San Diego, CA, 1990.

(12) Aksay, I. A.; Trau, M.; Manne, S.; Honma, I.; Yao, N.; Zhou, L.; Fenter, P.; Eisenberger, P. M.; Gruner, S. M. *Science* **1996**, *273*, 892–897.

(13) Yao, N.; Ku, A. Y.; Nakagawa, N.; Lee, T.; Saville, D. A.; Aksay, I. A. *Chem. Mater.* **2000**, *12*, 1536–548.

(14) Dabbs, D. M.; Aksay, I. A. *Annu. Rev. Phys. Chem.* **2000**, *51*, 601–622.

(15) Saville, D. A.; Chun, J.; Li, J.-L.; Schniepp, H. C.; Car, R.; Aksay, I. A. *Phys. Rev. Lett.* **2006**, *96*, 18301-1–18301-4.

(16) Miyata, H.; Kuroda, K. *Chem. Mater.* **1999**, *11*, 1609–1614.

(17) Miyata, H.; Kuroda, K. *Adv. Mater.* **1999**, *11*, 1448–1452.

(18) Trau, M.; Yao, N.; Kim, E.; Xia, Y.; Whitesides, G. M.; Aksay, I. A. *Nature* **1997**, *390*, 674–676.

(19) Yang, P.; Deng, T.; Zhao, D.; Feng, P.; Pine, D.; Chmelka, B. F.; Whitesides, G. M.; Stucky, G. D. *Science* **1998**, *282*, 2244–2246.

(20) Yamaguchi, A.; Uejo, F.; Yoda, T.; Uchida, T.; Tanamura, Y.; Yamashita, T.; Teramae, N. *Nat. Mater.* **2004**, *3*, 337–341.

(21) Wu, Y.; Cheng, G.; Katsov, K.; Sides, S. W.; Wang, J.; Tang, J.; Fredrickson, G. H.; Moskovits, M.; Stucky, G. D. *Nat. Mater.* **2004**, *3*, 816–822.

(22) Melosh, N. A.; Davidson, P.; Feng, P.; Pine, D. J.; Chmelka, B. F. *J. Am. Chem. Soc.* **2001**, *123*, 1240–1241.

(23) Hillhouse, H. W.; van Egmond, J. W.; Tsapatsis, M.; Hanson, J. C.; Larese, J. Z. *Chem. Mater.* **2000**, *12*, 2888–2893.

(24) Hillhouse, H. W.; Okubo, T.; van Egmond, J. W.; Tsapatsis, M. *Chem. Mater.* **1997**, *9*, 1505–1507.

(25) Edler, K. J.; Reynolds, P. A.; Brown, A. S.; Slaweck, T. M.; White, J. W. *J. Chem. Soc., Faraday Trans.* **1998**, *94*, 1287–1292.

(26) Kim, W. J.; Yang, S. M. *Chem. Mater.* **2000**, *12*, 3227–3235.

(27) Tolbert, S. H.; Firouzi, A.; Stucky, G. D.; Chmelka, B. F. *Science* **1997**, *278*, 264–267.

(28) Firouzi, A.; Schaefer, D. J.; Tolbert, S. H.; Stucky, G. D.; Chmelka, B. F. *J. Am. Chem. Soc.* **1997**, *119*, 9466–9477.

(29) Amundsen, K.; Helfand, E.; Quan, X. N.; Hudson, S. D.; Smith, S. D. *Macromolecules* **1994**, *27*, 6559–6570.

(30) Morkved, T. L.; Lu, M.; Urbas, A. M.; Ehrichs, E. E.; Jaeger, H. M.; Mansky, P.; Russell, T. P. *Science* **1996**, *273*, 931–932.

systems.<sup>31</sup> Polarization effects were also used to orient liquid crystals.<sup>32</sup> In general, high field strengths ( $E > 10^5$  V/m) are needed to produce orientation via polarization effects because of the relatively low dielectric contrast encountered in self-assembling organic systems. In systems with pre-existing charge, application of electric fields gives rise to *electrokinetic effects*, which typically scale linearly with the applied field strength and the free charge (i.e., electrophoresis and electroosmosis). A first-order electric field effect on orientation in block copolymers was demonstrated while electric fields applied to ceramic systems yielded only minor changes in shape and pore size distribution, consistent with electroosmotic flow (EOF) through the porous networks and accompanying anisotropic densification between the electrodes.<sup>33–35</sup>

With regards to surfactant-based systems, Trau et al. successfully combined high-strength electric fields ( $E \sim 10^5$ – $10^8$  V/m), confinement, and mold surface effects to produce nanoscopic silica patterned thin films with nanochannels oriented parallel to the field.<sup>18</sup> While these experiments demonstrated orientation, they did not distinguish between the contributions of confinement, mold surface, and electric field effects. Trau et al. hypothesized that the orientation was due, in part, to polarization effects, while EOF was responsible for filling the microcapillary channels.<sup>18</sup> Subsequently, Huang et al. found that electric fields substantially increased the length of silver and polyaniline nanowires synthesized in the water regions of reverse micelle liquid crystals with parallel orientation to the applied field.<sup>36,37</sup> Huang et al. attributed their observations to EOF by assuming that the previous work by Trau et al. provided a definite proof for an electrokinetic effect, specifically EOF, for the orientation, although this claim was not made by Trau et al. The goal of this paper is to clarify this ambiguity. Here, we show that EOF is indeed responsible for the orientation effects.

In order to clarify the role of the electric field in guiding the self-assembly of nanoscopic silica, we relax the confinement condition and find that electric fields orient nanoscopic silica, independent of other means of guiding the self-assembly. We explore the extent of the electric field effect and identify the mechanism in the low field strength regime. We also present evidence of a field-induced morphological restructuring from particles into fibers with aligned nanochannels. Furthermore, kinetic analysis of the restructuring process over a range of field strengths and synthesis conditions shows that the response is consistent with an electrokinetic mechanism. These results demonstrate that the electric field is more effective at producing orientation than previously thought.

## Experimental

**Methods.** We studied the electric field effect using the apparatus shown in Figure 1. Nanoscopic silica was grown from aqueous solutions containing cetyltrimethylammonium chloride (CTAC), tetraethoxysilane (TEOS), hydrochloric acid (HCl), and, optionally, sodium chloride (NaCl). Chemicals were obtained from Aldrich

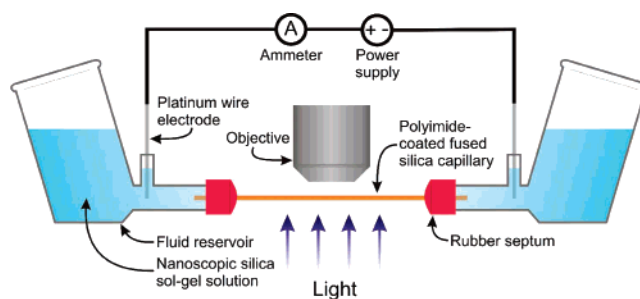


**Figure 1.** Schematic of experimental apparatus. A fused silica capillary, with a size ranging from 50 to 250  $\mu\text{m}$  ID is connected to fluid reservoirs. An electric field is applied through Pt electrodes inserted into the reservoirs. The growth process is monitored by mounting the entire cell on an optical microscope equipped with a video capture system.

and used as received. Typical precursor solutions contained 0.06–0.36 M CTAC, 0.06–1.08 M TEOS, and 0.55–1.6 M HCl (pH 0.26 to  $-0.2$ ).<sup>2</sup> For kinetic experiments, two compositions (“acid” and “salt”) were chosen to bring out the catalytic effects of acid while controlling the total ionic strengths of the solutions. Acid solutions contained 0.36 M CTAC and 1.08 M TEOS in 1.6 M HCl, and the salt solutions contained 2 M NaCl, 0.36 M CTAC, and 1.08 M TEOS in 0.55 M HCl. Fused silica capillaries with inner diameters (IDs) ranging from 50 to 250  $\mu\text{m}$  were obtained from Polymicro, Inc. and were used as received. Experiments were performed using capillaries with both round and square cross-sections. Square capillaries were preferred experimentally because the flat walls made it easier to obtain sharp optical images. The qualitative features of the response were independent of the capillary cross-section. Capillaries were flushed with a minimum of 5 times the capillary volume using the precursor solution before being connected to the reservoirs to rinse out any impurities and to systematize the walls before use.

In a typical experiment, the capillary was filled with precursor solution using a syringe and then connected to the fluid reservoirs. In the first set of experiments, the electric field was activated immediately. In the second set of experiments, the electric field was activated after a predetermined delay to allow particle formation. In both cases, direct current (DC) potentials ranging from 1 to 10 kV were applied through platinum electrodes inserted into the reservoirs with a spacing of about 10 cm. In this configuration, the applied electric field ranged from  $10^2$  to  $10^4$  V/m. Alternating current (AC) fields were also used, but no noticeable effects were observed at frequencies above 1 Hz. Lower frequencies were not examined. For each experiment, the in situ response of the material was recorded digitally using an optical microscope and computer workstation. Afterward, the capillary was removed from the apparatus, dried, calcined in air at 600  $^\circ\text{C}$  and examined using a scanning electron microscope (SEM) and small-angle X-ray scattering (SAXS) to determine the micron-level morphology and the orientation of the surfactant-templated nanochannels.

Experiments were performed using a Tektronix PFG5105 programmable pulse/function generator with a Trek 20/20 amplifier ( $\pm 20$  kV). To protect the amplifier from current overload, an 18 M $\Omega$  resistor was added in series to the electric circuit. The Tektronix PFG5105 signal generator was also used to perform a limited number of AC experiments. Experiments were performed using square, saw tooth, and sinusoidal wave forms and frequencies ranging from 1 to 100 MHz.

**Characterization.** The growth process was observed in real time by mounting the fluid cell on a Nikon Microphot-SA optical microscope with  $\times 50$ ,  $\times 100$ , and  $\times 200$  objectives. The microscope was equipped with a VHS video capture system. Digital images were then captured from the videotape using Global Lab Image 2 v.2.50 software (Data Translation, Inc.). For each image, six discrete particles (regions of interest, ROIs) were visually identified. The width and length of each ROI were manually measured and recorded. The average values of the width, length, linear displacement, and

(31) Körner, H.; Shiota, A.; Bunning, T. J.; Ober, C. K. *Science* **1996**, *272*, 252–254.

(32) Buka, A.; Kramer, L., Eds. *Pattern Formation in Liquid Crystals*; Springer: New York, 1996.

(33) Tsori, Y.; Tournilhac, F.; Andelman, D.; Leibler, L. *Phys. Rev. Lett.* **2003**, *90*, 145504-1–145504-4.

(34) Yuan, L.; Li, J.-F.; Viehland, D. *J. Am. Ceram. Soc.* **1995**, *78*, 3233–3243.

(35) Liang, K. M.; Huang, W. L.; Gu, S. R. *Mater. Res. Bull.* **2000**, *35*, 115–123.

(36) Huang, L.; Wang, H.; Wang, Z.; Mitra, A.; Bozhilov, K. N.; Yan, Y. *Adv. Mater.* **2002**, *14*, 61–64.

(37) Huang, L.; Wang, Z.; Cheng, X.; Mitra, A.; Yan, Y. *J. Mater. Chem.* **2002**, *12*, 388–391.

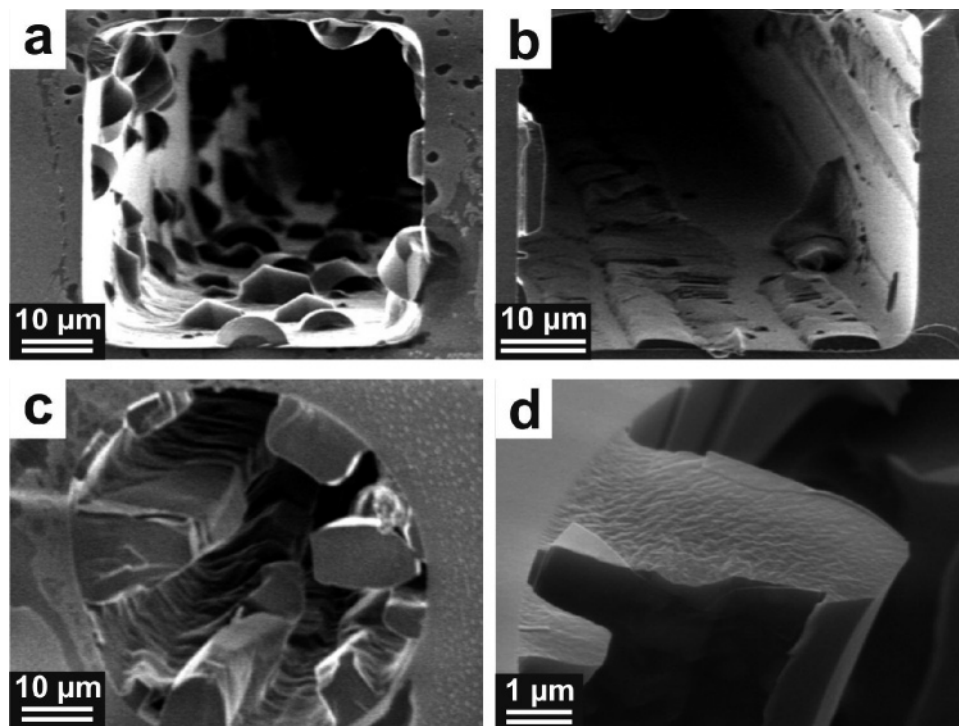


**Figure 2.** Cross-sectional SEM images of nanoscopic silica grown in fused silica capillaries. (a) In the absence of an electric field, the nanoscopic silica forms particles on the capillary walls. (b–d) Fibers are formed when an electric field is applied during growth. Similar features are observed in both square (b) and round (c,d) capillaries. The samples in the square capillaries (a,b) were prepared from a solution containing 0.06 M CTAC, 0.06 M TEOS, pH 0.26, and electric fields of 0 and 100 V/m, respectively. The samples in the round capillaries (c,d) were prepared from a solution containing 0.36 M CTAC, 1.08 M TEOS, pH 0, and an electric field of 100 V/m.

normalized elongation were recorded for each image. The process was repeated for multiple images at several time frames. The migration velocity was calculated from the slope of the displacement versus time plot. Since the boundaries of ROIs became increasingly difficult to identify as they merged into continuous fibers, the data collected during the early stages of migration were deemed more accurate than data collected at later stages. Careful examination of the large and small features in 10 videos gathered over a range of compositions and electric field strengths did not reveal a correlation between the size of the ROI and the migration rate. Attempts to automate the process were unsuccessful because the software was not able to reliably identify features. Instead, the position of the particle was taken to be the average of the front and back edges of the particle.

SEM images were obtained using a Philips XL-30 instrument at an accelerating voltage of 2–5 keV. The fused silica capillaries were sectioned into 1–2 mm segments using a razor blade and mounted vertically on an aluminum stub using carbon tape. The segments were coated with 2–5 nm of iridium to reduce sample charging and beam damage.

SAXS data were collected on the D1 beamline at CHESS (Cornell High-Energy Synchrotron Source), Cornell University. Synchrotron radiation was necessary because of the difficulty in obtaining a sufficiently strong scattering signal from the sample to determine the structure due to the small amount of scattering material (~10–100 ng) and the high level of background scattering from the silica capillaries. The high brilliance ( $10^{15}$  photons/sec/mrad<sup>2</sup>/mm<sup>2</sup>/0.1% bandwidth)<sup>38</sup> allowed the collection of quality images. Since the strength of the scattering signal is proportional to the mass of material to the 2/3 power,<sup>39</sup> efforts were made to increase the size of the

features formed by increasing the reagent loading in the precursor solution. The oriented sample analyzed here was prepared by infiltrating a 250  $\mu\text{m}$  ID capillary with a solution containing 0.24 M CTAC and 1.08 M TEOS in pH 0 water. After a 75 min nucleation delay, a 1 kV/m electric field was activated. The experiment was continued for 20 h, after which the capillary was dried, calcined, and mounted. A separate control experiment was performed without an electric field using the same precursor solution.

The signal-to-noise ratio was further improved by extracting an oriented fragment from the capillary. A  $500 \times 50 \times 20 \mu\text{m}$  ( $\sim 10$  ng) fragment was recovered by crushing a segment of capillary. The fragment was mounted orthogonally on the end of a fused silica capillary using a minimal amount of epoxy. Optical microscopy of the mounted sample showed that the long axis of the fragment coincided with the direction of the electric field during the synthesis process. The mounted fragment was scanned parallel and normal to the fiber axis. Regions in which strong diffraction spots occurred were located by translating the sample in the  $x$  and  $z$  directions in 100  $\mu\text{m}$  increments.

The control sample contained discrete nanoscopic silica particles in the capillary. To preserve any orientational order in the particles, a segment of the control sample capillary was mounted orthogonally on the end of a fused silica capillary. Scans were taken parallel and normal to the capillary axis. A more detailed description of the data acquisition procedure is included as Supporting Information.

The beam was tuned to 12.0 keV ( $\lambda = 1.033 \text{ \AA}$ ), and slits were adjusted to produce a  $150 \times 150 \mu\text{m}$  beam. Samples were mounted 25 cm from the CCD detector. The CCD camera had  $1024 \times 1024$  pixel resolution with a pixel size of  $50 \mu\text{m}$ . Acquisition times of 120, 200, and 500 s were used. Backgrounds collected over the same acquisition times were subtracted, and in-house corrections for the intensity and geometric distortions due to fiber optics in the detector were performed on-site. Helium-filled flight tubes with Kapton covers were used to reduce the scattering from air. Kapton produced weak diffraction rings spaced at  $q = 0.164 \text{ nm}^{-1}$  ( $d = 6.1 \text{ nm}$ ) and  $q = 0.328 \text{ nm}^{-1}$  (second-order ring).

(38) Zhou, X. S.; Lu, C. Q.; Millar, J. *Ind. Eng. Chem. Res.* **1996**, *35*, 2075–2090.

(39) For multislit diffraction, the signal intensity scales with  $N^2$ , where  $N$  is the number of slits. The number of slits is proportional to the cube root of the volume. Since the volume is proportional to the mass, the signal scales with  $V^{2/3}$ . The width of the peak varies as  $1/N$  or  $V^{-1/3}$ .

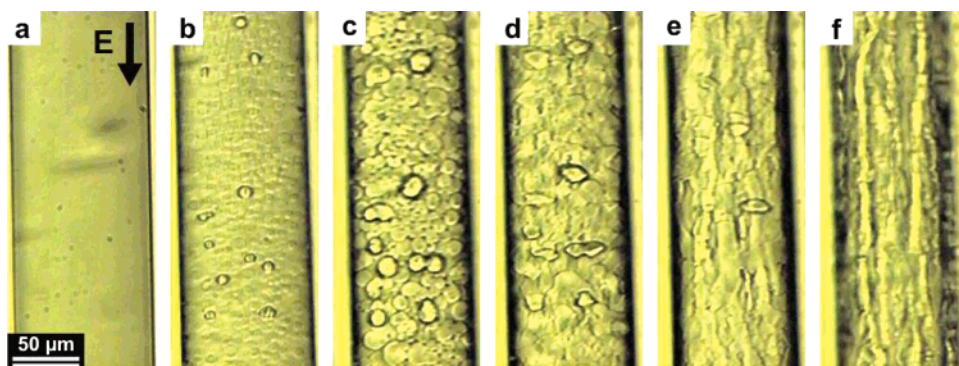


**Figure 3.** Structural evolution of nanoscopic silica under an electric field. A 2.2 kV/m electric field was activated 75 min after loading of a salt precursor solution into the capillary. Time-lapse optical images show the morphology of the nanoscopic silica at various times: (a) 20 min after loading, immediately before particle nucleation; (b) 25 min after loading, immediately after particle nucleation; (c) 74 min after loading, immediately before activation of the electric field; (d) 80 min after loading, 5 min after activation of the field; (e) 90 min after loading, 15 min after activation of the field; and (f) 195 min after loading, after the particle-to-fiber transition is complete.

## Results

Figure 2 shows SEM images of nanoscopic silica prepared with and without an electric field applied through the capillary. In the absence of the field, truncated cone-shaped features—reminiscent of gyroid-like particles—formed on the walls of the capillaries after the end of the nucleation period. In cases where the capillary diameter was sufficiently large (e.g., greater than 75  $\mu\text{m}$  for the solution compositions used), particles also formed directly in solution away from the walls through homogeneous nucleation. These particles either settled on to the wall or were flushed out of the capillary by convective flow due to pressure differences between the fluid reservoirs and due to electrophoresis as well under electric field. The cone-like features displayed random orientation with respect to the capillary axis and random distribution along the capillary wall. Particles that nucleated in the bulk and attached to the wall also did not exhibit a preferred orientation. In contrast, elongated fibers having cross-sections with well-defined corners formed when an electric field was applied during growth. The well-defined edges were seen in both control and field experiments, suggesting a common origin and a crystalline structure even at early stages of growth.<sup>13</sup> However, the exact reason for the edges is not known. Heat treatment did not cause any morphological changes, although, in some cases, the features detached from the wall after calcination due to densification of the silica matrix.

A series of optical images showing the growth of nanoscopic silica and its response to an electric field activated after particle formation is shown in Figure 3.<sup>40</sup> Initially, the capillary contained only the precursor solution. Particles nucleated and grew on the wall at the end of a nucleation period whose duration depended on the composition of the precursor solution.<sup>41</sup> The particle morphology was qualitatively similar to the particles seen in Figure 2 and independent of the capillary shape and diameter and the composition of the precursor solution. An electric field was activated a few minutes *after* particle formation. Under the influence of the field, the particles migrated toward the anode and merged with each other to form fibers. These fibers resembled the fibers that were produced when the field was activated *before* particle formation. The rate of migration increased with field strength and, for a given field strength, was faster in the salt composition since the presence of salt slowed the rate of

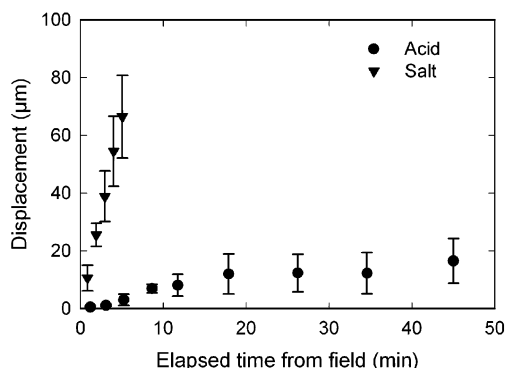


**Figure 4.** The average displacement vs elapsed time for salt ( $E \sim 780$  V/m) and acid ( $E \sim 370$  V/m) compositions at different field strengths. The electric field was activated after a 75 min delay.

polysilicate polymerization and thus the increase in the mechanical strength. Particles that nucleated in the bulk and had attached to the wall also underwent shape transition. Longer delays before field activation resulted in slower responses. At delays over 10 times the nucleation period, no response was observed. Similar qualitative behavior was observed at field strengths as low as 200 V/m, but the resulting fibers were not as straight as those shown in Figure 3.

The kinetic response of the particle (i.e., the center of mass displacement) to fiber transition was recorded for both the acid and salt compositions under a range of different field strengths and delays. The response was quantified in terms of the applied electric field strength, the field activation delay, and the reagent composition. This was accomplished by computing the initial migration velocity, mobility, and threshold field strength for each set of data. Figure 4 shows displacement data for two sets of experiments corresponding to rapid (salt composition,  $E \sim 780$  V/m) and slow (acid composition,  $E \sim 370$  V/m) kinetics. The average displacement of particles attached to the wall was a linear function of the elapsed time from the activation of the electric field regardless of the delay time, with the slope of the line being the initial displacement rate, as seen in Figure 5a. The initial displacement rates for a given composition and delay were plotted against the applied field strength, as shown in Figure 5b; the linear fit indicates a first-order field dependence. This allowed a mobility and threshold field strength to be defined according to  $u = \mu E + b$ , where  $u$  is the initial migration velocity,  $E$  is the field strength,  $\mu$  is the mobility, and  $b$  is a correction for the threshold field strength. The threshold field strength was computed from  $-b/\mu$ . Values for the mobility and threshold field strength

(40) A time-lapse movie showing the structural evolution for different precursor solution compositions and under different fields is available as Supporting Information.

(41) The nucleation period was 30 min for the salt composition and 20 min for the acid composition. Ku, A. Y. Ph.D. Thesis. Princeton University, 2004.

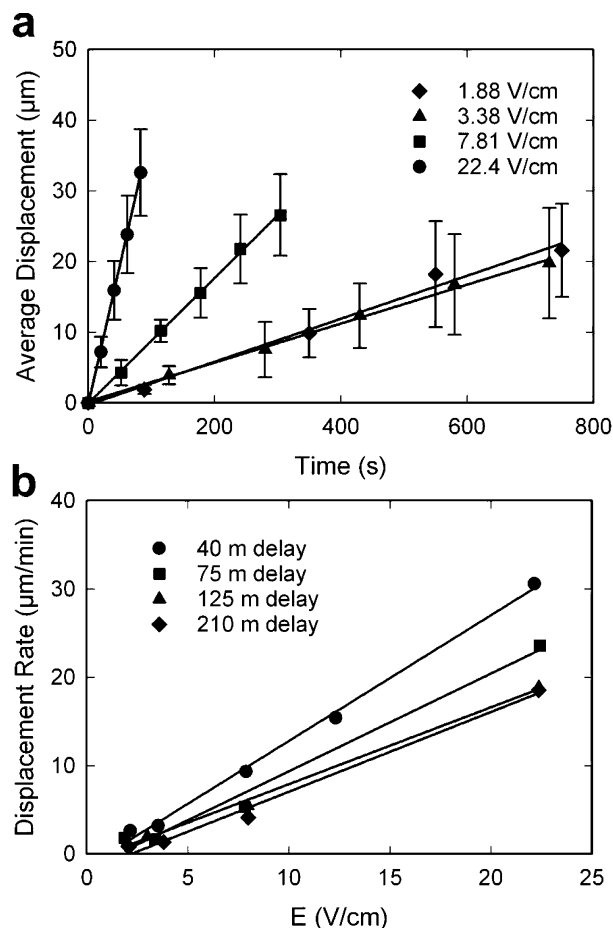


**Figure 5.** (a) The average displacement of the gyroid center of mass vs time for a 75 min delay at several field strengths. A linear regression was performed on each data set and used to determine the displacement rate vs field strength plot seen in panel b. Similar plots were performed for delay times of 40, 125, and 210 min. (b) The displacement rate vs applied field for salt compositions and delays of 40, 75, 125 and 210 min. The lines are linear fits to the data.

**Table 1. Numerical Estimates of the Mobility, Intercept, and Threshold Field Strength**

	acid			salt			
delay (min)	40	75	125	40	75	125	210
mobility, $\mu$ , ( $\mu\text{m}\cdot\text{cm}/\text{V}\cdot\text{min}$ )	0.24	0.15	0.054	1.4	1.1	0.88	0.90
intercept, $b$ , ( $\mu\text{m}/\text{min}$ )	-0.33	-0.70	-0.35	-1.2	-1.5	-0.94	-1.9
threshold field (V/m)	140	490	650	85	140	110	210

are listed in Table 1. In general, the mobility decreased with the increasing delay, while the threshold field strength increased. In the limit of long delay times, no restructuring occurred. Similarly, no response was noticeable for field strengths less than about 100 V/m.

The micron-level shape change was accompanied by a nanometer-level change in the orientation of the surfactant-templated nanochannels, as confirmed by SAXS. Figure 6 shows synchrotron SAXS patterns from a sample restructured by an electric field and a control sample. Scans were taken in two orthogonal directions. In the electric-field-treated sample, the scattering patterns showed 6-fold and 2-fold symmetry when the X-ray beam was oriented parallel and normal to the fiber axis, respectively. These scattering patterns are consistent with an array of hexagonally packed cylinders oriented parallel to the

field. A hexagonal set of arcs corresponding to a  $d_{100}$  spacing of 30 Å was observed when the beam was parallel to the fiber. The angular full width at half-maximum (fwhm) of the arcs was 17°, suggesting good registry of the hexagonally packed channels. The mosaicity compares well with the result of 20° previously obtained for material grown under conditions identical to those reported by Trau et al.<sup>42</sup> When the beam was oriented normal to the fiber axis, oppositely spaced arcs corresponding to a  $d_{100}$  spacing of 28 Å were observed. The angular fwhm of the arcs ranged from 69° to 78° depending on the location at which the sample was scanned. The relatively broad angular mosaic suggests a preferred, but not perfect, orientation of the nanochannels parallel to the electric field direction. This may have been due to the incomplete alignment of the domains by the electric field. Furthermore, the presence of peaks within the opposite arcs indicated partial, but not complete registry of the domains. Despite the mosaicity in the parallel (~17°) and perpendicular (~70°) orientations, the SAXS data provide direct evidence of field-induced orientation of nanochannels parallel to the electric field direction. In contrast, the scattering patterns from the control sample exhibited first-order diffraction rings, corresponding to a  $d_{100}$  spacing of 27 Å, in both scan directions. No diffraction spots were observed in any of the scans, indicating a lack of orientational order between the particles attached to the capillary walls. Higher order scattering rings were not observed because the scattering from the sample was weak due to the small amount of material present and the background scattering from the fused silica capillary.

## Discussion

In attempting to isolate the role of the electric field, it is important to recognize that the nanoscopic silica fibers may be subject to confinement, surface registry effects, and shear during experiments. However, in our experiments, none of these effects is expected to contribute significantly to the alignment process. Physical confinement of the nanoscopic silica particles was minimized by performing experiments in capillaries with diameters larger than the natural size of the particles. This enabled the particles and fibers to attain their “natural” length scale, as evidenced by the consistent size and shape of the features in capillaries of different size and shape. Surface registry effects could not be completely eliminated because of the tendency of surfactant channels to organize parallel to the capillary walls, but were minimized through the use of amorphous walls.<sup>12</sup> This is confirmed by the absence of particle orientation in the SEM and SAXS data under control conditions. Shear was also discounted as a factor in the orientation using a series of control experiments in which a pressure-driven background flow was imposed by slightly increasing the fluid level in one of the reservoirs. Although the background flow was sufficient to flush some particles out of the capillary, it did not alter the shape of the particles attached to the wall in the control experiments. In all cases, the electric-field-induced migration of silica was in the direction of the anode, independent of the direction of the background flow. Together, these observations indicate that the electric field is solely responsible for the orientation.

Several features of the response suggest that low-strength electric fields affect the structure through an electrokinetic rather than polarization-based mechanism. First, the restructuring rate is linearly dependent on the field strength, as seen in the mobility plots, while polarization effects typically scale with the square of the applied field strength.<sup>43</sup> The first-order dependence is

(42) Zhou, L.; Fenter, P.; Dabbs, D. M.; Eisenberger, P. E.; Aksay, I. A., Princeton University, Princeton, NJ. To be submitted to *Langmuir* for publication.

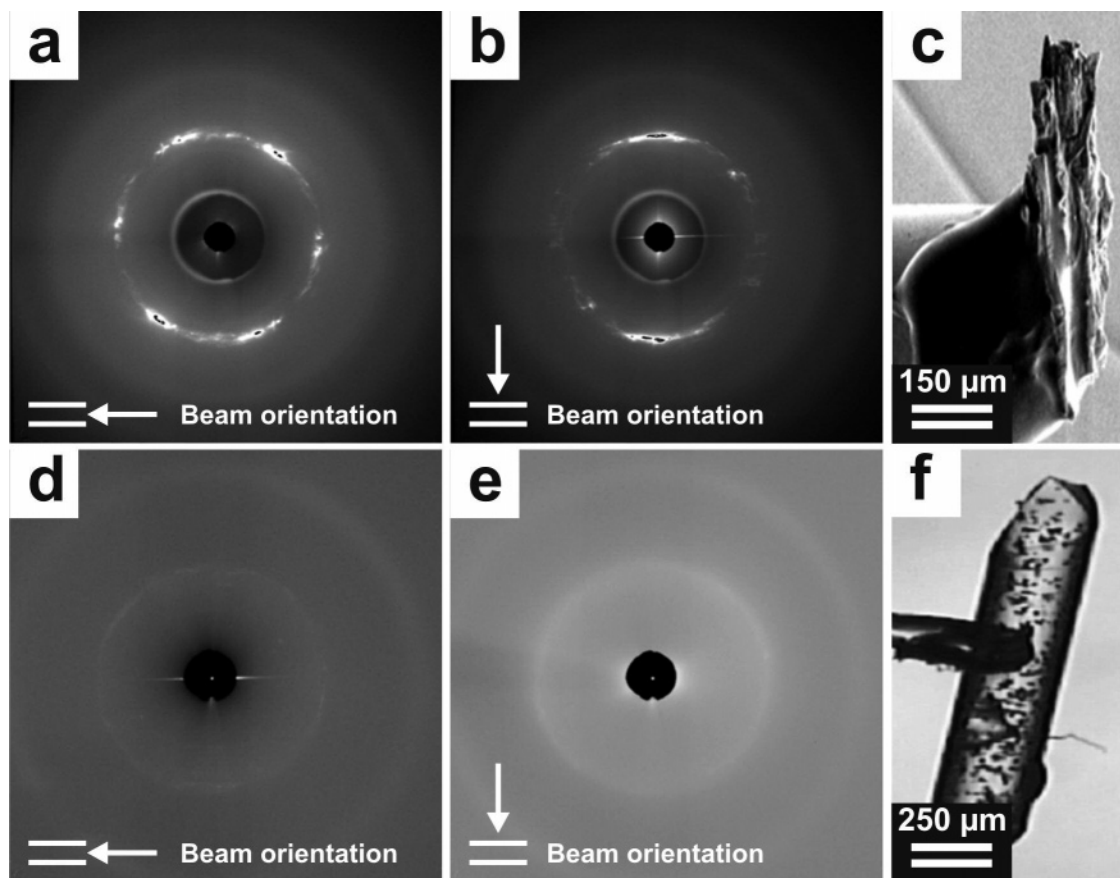


**Figure 6.** Electric-field-induced orientation in nanoscopic silica. SAXS patterns collected parallel and normal to the capillary axis for a sample treated with an electric field (a,b) and a control sample (d,e). The dark spots in the center of some of the arcs represent high-intensity peaks at which detector overflow occurred. The faint outer rings are reflections from the Kapton tape used to suspend the beam stop. The arcs that intersect the beamstop in the pattern (d) are due to reflections off of the capillary walls. Both samples were prepared in a 250  $\mu\text{m}$  round capillary using a salt precursor solution. A 1 kV/m electric field activated after a 40 min delay was used to produce oriented fibers, which were extracted from the capillary and glued to a mount before examination. Images of the mounted oriented fiber (c) and the control sample (d) are also shown. The particles in the control sample were not extracted because they could not be removed from the capillary without loss of orientational registry.

further corroborated by correlation between the direction of the migration and the polarity of the field and the absence of a response to AC fields. For the case of positively charged micelle and silica surfaces, electrokinetic flow arises due to the action of the electric field on the mobile anions. This flow is in the direction of the anode, which is consistent with the observed behavior. Second, the effect described here was observed at field strengths as low as 200 V/m, about 3 orders of magnitude lower than the field strength typically needed to produce polarization-based orientation where field strengths of  $10^5$ – $10^8$  V/m are common.<sup>29,32</sup> These features may be due in part to the presence of charged surfactants in the precursor solution. Since previous attempts to affect the structure of ceramics produced through sol–gel methods using electric fields have only resulted in minor changes in the shape and the pore size distribution,<sup>34,35</sup> the charge introduced by the surfactant may be responsible for the electrokinetic effect. The polarity of the response is consistent with anion motion, suggesting that the orientation is due to the EOF in the electrical double-layer near the positively charged surfactant or the EOF of the chloride counterions associated with the silicate protonation.

The data in Table 1 can be interpreted in terms of the mechanical response of the silica matrix to stresses produced by the electric field. The rate of restructuring is expected to vary with the mechanical rigidity of the silica matrix. Over time, the silica

matrix becomes more rigid due to the formation of covalent bonds through acid-catalyzed condensation reactions.<sup>11,16</sup> This qualitatively accounts for the trends in Table 1. First, the higher rate of condensation in acid compositions results in lower mobilities relative to the corresponding values for the salt compositions. Second, the monotonic decrease in mobility with increased delay times follows from the increasing resistance of the silica matrix to deformation. Finally, the threshold field strength increases with time, also as a result of the increased mechanical strength of the silica matrix.

Over the field strengths ( $10^2$ – $10^4$  V/m) used in this work, electrokinetic effects appear to be responsible for orientation. Higher field strengths were not examined because our power supply could not sustain the necessary current at those field strengths. The absence of kinetic data at the field strengths used by Trau et al. ( $E \sim 10^5$ – $10^8$  V/m) makes it impossible to rule out polarization effects in the high field strength regime.<sup>18</sup> Another factor that becomes important at higher field strengths is Joule heating. Since energy produced scales with the product of the current and the applied voltage, significant heating of the nanoscopic silica system may occur at higher field strengths. As Trau et al. pointed out, this may accelerate the sol–gel process, leading to more rapid stiffening of the silica matrix. However, it may also impact the equilibrium phase behavior of the surfactant template leading to a thermotropic rearrangement of the organized nanochannels.

(43) Landau, L. D.; Lifshitz, E. M.; Pitaevski, L. P. *Electrodynamics of Continuous Media*; Pergamon: Oxford, 1984.

### Conclusions

We have shown that guided self-assembly with low-strength ( $\sim 200$  V/m) electric fields provides a viable method for producing nanoscopic silica fibers with oriented nanochannels. Similar structures can also be obtained by applying an electric field shortly after the formation of nanoscopic silica particles. Quantitative analysis of the restructuring indicates these structural changes occur through an electrokinetic rather than polarization mechanism. The distinction is important, as electrokinetic phenomena arise from the action of a field on free charge, making it possible to orient the structure using relatively weak fields when charged surfactants are used as templates. We thus propose that the restructuring and orientation occur via the EOF derived from the motion of negative counterions. This effect expands the range of structures possible through guided self-assembly processes and is expected to be useful for preparing nanoporous silica with pores suitably oriented for microelectronic devices and membranes.

**Acknowledgment.** Financial support for this work was provided by MRSEC NSF/DMR-0213706 and ARO-MURI under Award No. W911NF-04-1-0170. We are grateful to K. J. Tatum and J. Chun for carefully reviewing and assisting with the preparation of this manuscript. We also thank E. Fontes, M. W. Tate, S. M. Gruner, and W. D. Ristenpart for help in analyzing the SAXS data. We are also grateful to G. W. Scherer for the use of his optical microscope. SAXS work was conducted at the Cornell High-Energy Synchrotron Source, which is supported by the National Science Foundation.

**Supporting Information Available:** Time-lapse video clips showing the structural evolution of samples prepared under various conditions (composition, field activation delay, and applied field strength) and a detailed description of the SAXS sample preparation and data acquisition procedures. This material is available free of charge via the Internet at <http://pubs.acs.org>.

LA0636154